

Contactless high frequency inductive position sensor with DSP read out electronics utilizing band-pass sampling

Bernhard Aschenbrenner, Bernhard G. Zagar

Institute for Measurement Technology, Johannes Kepler University, 4040 Linz, Austria

ABSTRACT

This paper presents a precise, reliable, low cost and contactless inductive absolute position measurement system for rough industrial environments. It offers a high inherent resolution (0.04 % of antenna length), and measures absolute position over a relative wide measurement range. The main property for this kind of sensor is its good immunity to external noise and target misalignment off the measurement axis. The measurement range and the precision are extended by adding additional and finer pitched receive coils. This sensor works on similar principles as resolvers but consists of a rectangular antenna PCB, a small moveable passive LC resonant circuit and a signal processing unit. Furthermore, the used read out electronics utilizes under-sampling to demodulate the sensor output signals and the corresponding position is estimated from a lookup table (LUT) implemented on a digital signal processor (DSP) to avoid singularities in the inverse tangent and cotangent calculation. Moreover, the mechanical transducer arrangement, the signal condition electronics design and measurement results of the transmitter to receiver signal coupling and relative position error will be presented.

Section: RESEARCH PAPER

Keywords: inductive sensor; contactless; band-pass-sampling; synchronous demodulation, resonant circuit

Citation: Bernhard Aschenbrenner, Bernhard G. Zagar, Contactless high frequency inductive position sensor with DSP read out electronics utilizing band-pass sampling, Acta IMEKO, vol. 3, no. 3, article 11, September 2014, identifier: IMEKO-ACTA-03 (2014)-03-11

Editor: Paolo Carbone, University of Perugia

Received February 15th, 2013; **In final form** April 10th, 2014; **Published** September 2014

Copyright: © 2014 IMEKO. This is an open-access article distributed under the terms of the Creative Commons Attribution 3.0 License, which permits unrestricted use, distribution, and reproduction in any medium, provided the original author and source are credited

Funding: This work was supported by the Austrian Center of Competence in Mechatronics (ACCM)

Corresponding author: Bernhard G. Zagar, bernhard.zagar@jku.at

1. INTRODUCTION

Many industrial applications demand for precise absolute position measurement of objects placed in a harsh environment. Sensors for industrial applications have to meet criteria such as reliability, small size, wide temperature ranges, and insensitivity to moisture, vibrations, dust, chemicals and mechanical offset even in rough conditions. Ideally, the measurement system should fulfill these criteria without any mechanical contact to maintain long service life and should be applicable for highly dynamic drives. Prime candidates to meet these requirements are contactless inductive sensors. One of these inductive sensors is based on inductive resonance [1–4].

The developed sensor [5] can be used for absolute position measurement and measures the position accurately right from power up. This sensor works on a similar principle to contactless resolvers and utilizes the mutual inductance between an elongated antenna on a printed-circuit-board (PCB) and a target which acts as a passive LC resonant circuit. Figure 1 shows a sketch of the principle of operation.

The target is a passive high-Q LC resonant circuit with a planar rectangular inductance (L_T) formed by tracks on a PCB and a discrete capacitance (C_T). Furthermore, the antenna PCB contains five different planar coils which operate as transmission and receive circuits (see Figure 2 and Figure 3). The sine and cosine shaped coil pair with the single period over the full antenna PCB length l_A is used for absolute position measurement.

Already developed and used contactless high frequency inductive position sensors use a single pair of receive coils only and are thus not able to attain such a good resolving power [1,4,6].

Through adding two additional sinusoidal shaped receive coils with a shorter cycle length, the measurement precision and measurement range can be increased. However, these multi-cycle coils are only able to generate an incremental position signal and thus a more elaborate signal processing is necessary which is performed by a digital signal processor (DSP).

The envelopes of the amplitude modulated double sideband suppressed carrier (DSBSC) receive coils output signals contain the position information of the target. These voltages are

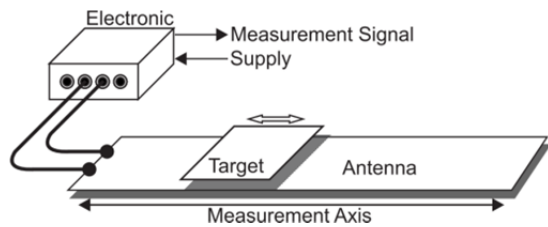


Figure 1. The picture shows a contactless inductive position sensor in linear arrangement, consisting of an antenna PCB, a target PCB which is a movable, passive, high-Q LC resonant circuit and a signal conditioning electronic.

amplified in an analog front-end, analog to digital converted, and digitally demodulated to calculate the position using the DSP. This way the measurement system attains an update rate of approximately 60 kHz.

Conventional resolver-to-digital converters seem to be ideal for high-frequency inductive position sensors but the carrier frequency of these converters, which is usually set between 2 and 30 kHz, is too low for the intended application of the sensor. In [1-3], an ASIC front end was developed for this kind of sensor which demodulates, amplifies and filters the DSBSC signals from the receive coils, offers a differential mixer topology for suppressing common mode voltages and provides an excitation voltage that supplies the transmitter coil. However, this ASIC cannot simultaneously sample the four receive coil signals, which is necessary for fast moving objects requiring high update rates.

After this introductory part, section 2 describes the basic theory of operation for this kind of sensor. In section 3 the problem of the transmitter-to-receiver coupling is described by a simple model and measurement results are shown. Section 4 describes the demodulation method of the received sensor signals utilizing band-pass-sampling. Section 5 gives an overview of the already developed signal conditioning electronics, the measurement setup and measurement results. Finally, conclusions are suitably drawn in Section 6.

2. OPERATING PRINCIPLES

The inductive position sensor operating principle is similar to the resolver operating principle. However, instead of a rotor winding and two stator windings there are an excitation coil and further four receive coils on the same antenna PCB. Furthermore, the coils are planar on the antenna PCB instead of a spatial arrangement like the resolver windings in a motor stator.

A typically planar arrangement of tracks which forms transmission and receive coils is illustrated in Figure 2. The absolute receive coil cycle length is $l_A = 390$ mm, and consequently the theoretical measurement range is $l_{th} =$

390 mm. Furthermore, the vernier multi-cycle receive coils contain 10 cycles with cycle length $l_p = 40$ mm, and its overall length is 400 mm. Thus, the total length of the vernier circuits is 10 mm longer than the absolute receive coils, due to via placing reasons at the right most end of the antenna PCB. Hence, the precise receive circuits have a cycle period of $l_p = l_A / 9.75 = 40$ mm. Furthermore, the single cycle receive coils have a width of 17 mm, the multi-cycle receive coils have a width of 18 mm, and the antenna PCB width is 26 mm. The transmission coil is formed by tracks which extend around the periphery of the antenna PCB forming three loops. The sine shaped tracks are the receive coils. All traces have a width of 0.254 mm on the antenna and target PCB, and the copper coating is 35 μ m thick on both PCBs.

The number of cycles is chosen such that the sensor resolution improves significantly and that the absolute coil signals detect the correct incremental index reliably.

As already mentioned the target LC resonant circuit is a simple passive and serial LC resonant circuit where the inductance L_T is a multilayer planar coil which is formed by a set of straight conductive tracks on a PCB, which can be seen in Figure 3. Targets are relatively short as compared to the antenna PCB and are typically attached to a moving host component.

The two single cycle coils of the antenna PCB are used to determine the absolute position and the multi-cycle windings improve the sensor resolution but are incremental. Thus, the single cycle or absolute coils must resolve smaller displacements than half the period of the multi-cycle coils to obtain the correct incremental index. Consequently, the determined multiple of the multi-cycle period length plus the relative target position delivers the precise and absolute position. Hence, the combination of two different pitches improves the sensor for high resolution position measurement.

Usually, a sine or square wave signal supplies the rectangular transmission coil which has a frequency range between 100 kHz and 4 MHz where the fundamental oscillation can be represented as $U_{Tx} = A_{Tx} \sin(2\pi f_0 t)$, where A_{Tx} and f_0 are the amplitude and the fundamental frequency of the excitation signal [1,2]. In the region of the transmission coil, a uniform, elongated and alternating electromagnetic field is formed due to the excitation signal.

When the target enters this alternating field, currents are induced to flow in the resonant circuit. These currents generate their own magnetic field, which induces a voltage in the receive coils. The magnetic coupling between the resonant circuit and each of the sensor receive windings varies with position, so that by applying an oscillating signal to the excitation winding at the target resonant frequency, a signal is induced in the four receive windings which oscillates at resonant frequency but whose amplitude varies as a function of the target position relative to

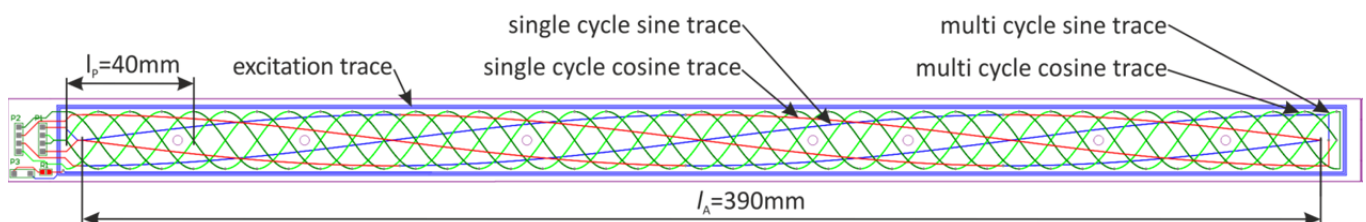


Figure 2. In the antenna PCB picture can be seen the transmission / excitation coil and the different sine and cosine structures which are manufactured on a four layer PCB and offers a theoretical absolute measurement length of 390 mm. The two single cycle sine and cosine structures are for absolute position measurement and the multi-cycle sine and cosine structures are for increased precise position measurement.

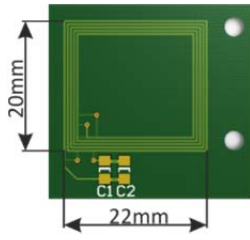


Figure 3. Resonant target PCB with the rectangular planar coil windings to form the inductance for the serial LC resonant circuit.

the antenna PCB. Because of the sine shaped receive coil design, the carrier signals are in phase with each other but the complex envelopes are in-phase and quadrature as a function of the target-position along the antenna PCB.

Theoretically, the two amplitude modulated receiver signals from the absolute structure can be represented in the time domain as follows:

$$U_{Acos}(t) = \frac{A_A}{2} \cos\left(\frac{2\pi x(t)}{l_A}\right) \sin\left(\omega t + \frac{\pi}{2}\right) + C_{Acos}(t), \quad (1)$$

$$U_{Asin}(t) = \frac{A_A}{2} \sin\left(\frac{2\pi x(t)}{l_A}\right) \sin\left(\omega t + \frac{\pi}{2}\right) + C_{Asin}(t), \quad (2)$$

where $x(t)$ is the absolute position of the target along the measurement axis, l_A is the cycle length of the absolute position coil, $\omega = 2\pi f$ is the angular frequency of the target resonance and excitation signal frequency and $C_{Acos}(t)$ and $C_{Asin}(t)$ are the capacitive coupling terms directly from the transmission to the absolute position windings [1,2].

The two amplitude modulated receive coil signals from the multi-cycle structure can be represented in the time domain as follows:

$$U_{Pcos}(t) = \frac{A_p}{2} \cos\left(\frac{2\pi x(t)}{l_p}\right) \sin\left(\omega t + \frac{\pi}{2}\right) + C_{Pcos}(t), \quad (3)$$

$$U_{Psin}(t) = \frac{A_p}{2} \sin\left(\frac{2\pi x(t)}{l_p}\right) \sin\left(\omega t + \frac{\pi}{2}\right) + C_{Pcos}(t), \quad (4)$$

where l_p is the pitch of the multi-cycle windings and $C_{Pcos}(t)$ and $C_{Psin}(t)$ are the capacitive coupling terms directly from the transmission to the multi-cycle receive windings.

The target position is determined from the relative amplitudes of the components of the signal induced in the sensor windings corresponding to the in-phase and the quadrature signal. If the signal pairs are doubled or halved, the calculated position remains unchanged. This ratiometric format yields immunity to variations in the excitation, multiplicative disturbances, temperature, and the sensitivity of the processing electronics.

The high operation frequency allows to avoid ferromagnetic coupling elements that in alternative designs can cause hysteresis effects thus decreasing both resolution and precision especially if an extended temperature range is demanded. Furthermore, without the target circuit there are no induced currents in the receive windings, because the conducting tracks of the sine and cosine receive coils are twisted properly. Therefore, the electrical current induced by the excitation field to flow in one loop of a receive coil is canceled out by an equal and opposite in phase induced current of the other loop. Using such twisted coils has the advantage that the influence of inductive crosstalk from the excitation coil current and by external electromagnetic noise is significantly reduced, if the number of loops is even [7,8].

A further main property of the ratiometric transducer design offers a greatly reduced influence of mechanical tolerances such as gap variations between target and antenna PCB or target displacements lateral to the measurement axis. Therefore, lateral misalignment variations to the measurement axis within $\pm 10\%$ of the sensor affect the measurement result only marginally because this invariance results from equal signal reduction in channel signals generated by the oscillating target [9].

The vertical distance between stator and target PCB depends on the application and is usually between 0.5 mm and 3 mm [1, 2].

The two single period receive windings offer absolute position measurement, but the effective measurement length should be limited to 80% of the structure length l_A to avoid edge effects. The system allows resolutions of 0.1% to 0.01% of the antenna length and the absolute linearity of the transducer is between 0.1% and 1% [4].

3. CAPACITIVE CROSSTALK

If there are two or more electrical circuits, there will be a capacitive coupling between them and if there are two or more current loops, there is an inductive coupling between each of them [8,11].

The geometry of the printed circuit board traces has to be such as to avoid to the greatest extends any of these unwanted coupling mechanisms. Since the sensor principle relies on the wanted inductive coupling effect due to the target PCB influence any unwanted cross-talk, be it inductive or capacitive is deteriorating sensor performance. Especially this sensor design suffers from the direct capacitive transmission to receive coil crosstalk, and this influences the linearity of the arc-tan ratio significantly [1, 2], whereas the inductive transmission to receive coil crosstalk is strongly suppressed by the receive circuit design as already explained in the previous section.

Figure 4 illustrates the amplitudes due to direct inductive transmission to receive coil crosstalk in dependence of the frequency and absence of the target PCB. The signals were measured for each receive winding by an impedance / gain phase analyzer (HP 4194A), which also supplied the excitation signal (a 2.4 V peak-to-peak sine wave). The receive windings were shorted out one after another and the induced currents were measured by a Tektronix TCP312 current clamp and a Tektronix TCPA300 amplifier.

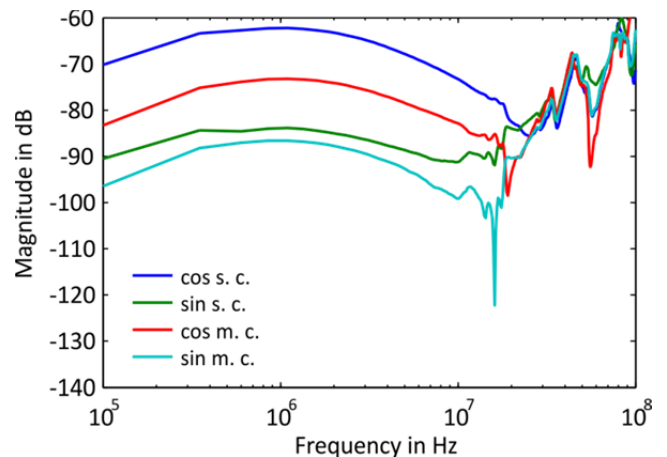


Figure 4. The plot shows the i_m/i_{Tx} , $m = \{Asin, Acos, Psin, Pcos\}$ behavior of the four receive windings due to direct inductive transmitter to receive coupling. i_{Asin} and i_{Acos} are the single cycle coil currents, i_{Psin} and i_{Pcos} are the multi-cycle coil currents and i_{Tx} is the excitation current.

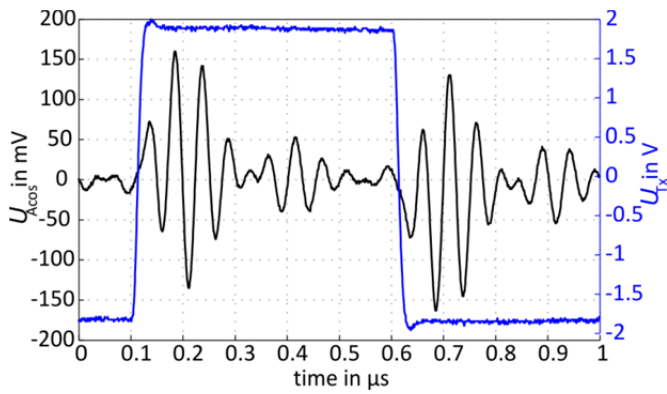


Figure 5. The measured coupling voltages on the absolute sine receive coil show voltage transients of 150 mV amplitude. The excitation voltage is approximately a 4 V peak-to-peak 1 MHz square wave signal.

It is easy to see, that the coupling is rather weak and the sine windings suppress the inductive coupling current even better by 15 to 20 dB than the cosine windings. Furthermore, the multi-cycle cosine receive winding offers a better suppression characteristic than the cosine single cycle winding, as well as the sine multi-cycle winding, due to the smaller loop areas which improves the crosstalk current cancellation. Moreover, the better suppressed amplitudes of the sine circuits results from the better receive circuit symmetry (see Figure 2). This happens because the multi-cycle and single cycle cosine windings contain loops with larger surfaces at the antenna leftmost position than the loops at the rightmost position. These differences occur due to the connection traces from the cosine windings to the connector P2.

Capacitive coupling can be separated as a first approximation from inductive terms by using open-loop measurements thus limiting current loops. The voltage due to capacitive coupling (see coupling terms in equations (1), (2), (3) and (4)) appears in phase with the induced voltages U_{Asin} , U_{Acos} , U_{Psin} and U_{Pcos} due to the target oscillating field. Because of this capacitive crosstalk, an offset voltage appears after demodulation, and thus, the linearity of the arc-tan ratio becomes distorted.

These capacitive transmitter-to-receive crosstalk voltages are shown in Figure 5 and Figure 6 for a square and a sine wave excitation signal in absence of the target PCB. The square wave excitation signal causes significantly higher disturbances than the sine wave excitation due to the higher harmonics of the square wave signal fundamental frequency ($3f$, $5f$, $7f$,...). Therefore, a sinusoidal excitation is recommended although a square

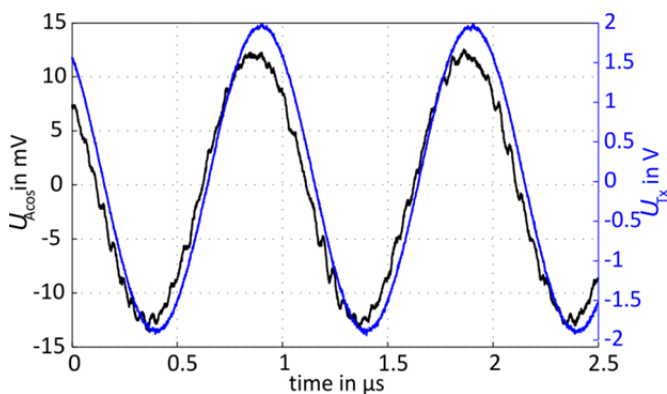


Figure 6. The measured coupling voltages on the absolute sine receive coil show voltage transients of 15 mV amplitude. The excitation voltage is approximately a 4 V peak-to-peak 1 MHz sine wave signal.

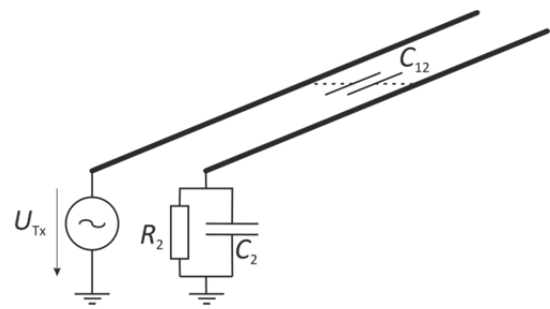


Figure 7. Simple model to describe the capacitive coupling between two parallel conductors.

wave signal is more simply to generate.

To describe this phenomenon theoretically, Figure 7 shows two PCB traces in close proximity. One trace is supplied by a sinusoidal voltage source, $u_{Tx}(t) = U_{Tx} \cdot \sin(\omega t)$ and the other trace is connected to ground via a resistor R_2 and a parallel capacity C_2 .

Furthermore, a transfer function which describes the coherent capacitive interference between these two parallel conductors illustrated in Figure 7 is given in [10] and can be used as a simple mathematical model to describe the capacitive coupling (C_{12}) between transmitter and receive coils. The transfer function for the coherent interference to any receive coil is given by:

$$\frac{U_{Rx}}{U_{Tx}}(s) = \frac{s C_{12} R_2}{s(C_{12} + C_2)R_2 + 1} \quad (5)$$

where C_{12} is the capacitance between the transmission and receive coils, which picks up the interference from the transmission coil. Resistance R_2 and capacitance C_2 are parallel-connected, and C_2 is the capacitance with respect to ground and R_2 the ohmic receive coil resistance. The variable U_{Rx} represents the crosstalk voltages from each receiver channel (U_{Asin} , U_{Acos} , U_{Psin} and U_{Pcos}) and is measured across R_2 . C_{12} is typically on the order of 2.3 pF to 3.1 pF for the single- and multi-cycle coils, C_2 is on the order of 17 pF, and R_2 is approximately 1.8 Ω for the single and approximately 2.8 Ω for the multi-cycle receive coil.

From inspection of equation (5), it is easy to see that in order to minimize the voltage U_{Rx} , due to capacitive crosstalk for all $\omega > 0$, C_{12} , R_2 and U_{Tx} have to be small. However, the coupling capacity C_{12} is difficult to reduce due to the closely spaced transmission and receive coil arrangement, and increasing the distance between the excitation and receive coils will increase the dimensions of the antenna PCB in width and length. The ohmic resistance can be reduced by reducing the number of vias (two layers a receive coil) and choosing thicker copper layers.

In Figure 8 the Bode diagram shows the capacitive transmitter-to-receive coil crosstalk behavior of the four receive windings in absence of the target PCB. The capacitive crosstalk behavior was measured for each receive coil one after another by an impedance analyzer (HP 4194A), which supplied the excitation signal of a 2V peak to peak sine wave. The frequency was swept from 100 kHz to 100 MHz. The receive coils are assumed unloaded.

In Figure 8 is easy to see that the voltage at the receive coils due to capacitive crosstalk increases with increasing frequency with approximately 20 dB per decade from 100 kHz to 10 MHz. Between 20 and 30 MHz is a resonance peak and for frequencies beyond 30 MHz the crosstalk decreases again. The

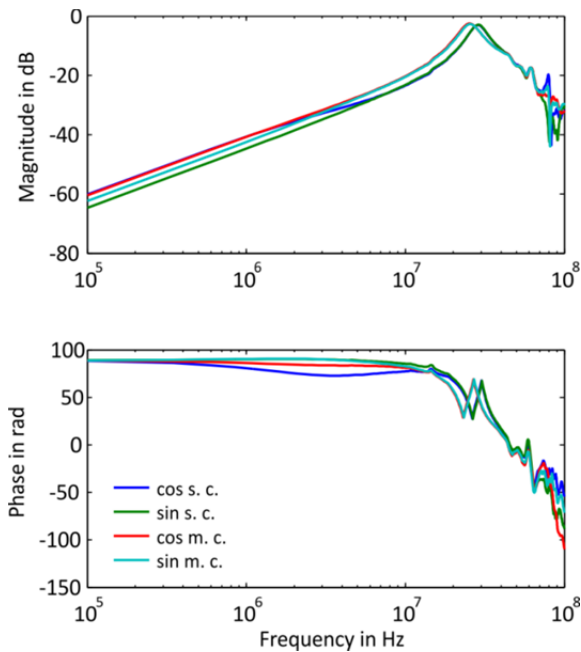


Figure 8. The Bode diagram shows the capacitive crosstalk behavior from the excitation winding to each of the four receive channels.

cause for this phenomenon is under research and cannot be explained yet. Therefore, equation (5) describes well the crosstalk behavior of this kind of sensor in the usual operating range between 100 kHz and 4 MHz.

The cosine coils exhibit stronger crosstalk than the sine coils due to edge effects (straight traces at the Antenna PCB ends)

4. AMPLITUDE DEMODULATION BY UNDERSAMPLING

For obtaining the position of the target, the two absolute receiver signals $U_{A\sin}$ and $U_{A\cos}$ (equation (1) and equation (2)) and precise receive signals $U_{P\sin}$ and $U_{P\cos}$ (equation (3) and equation (4)) have to be demodulated to extract the envelope from the DSBSC receiver signals. The amplitude modulated receiver signals can be demodulated by using any synchronous demodulating technique.

One basic method utilizing digital demodulation is introduced in this section. The $U_{A\sin}$, $U_{A\cos}$, $U_{P\sin}$ and $U_{P\cos}$ signals are sampled at the same frequency as the carrier frequency f . This, so called under-sampling, synchronously demodulates the

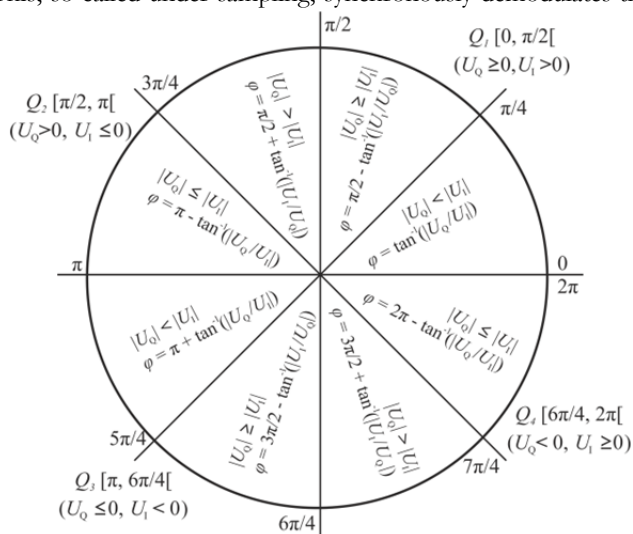


Figure 9. Arc-tan computation for measurement range $[0, 2\pi x/l_A]$ [8].

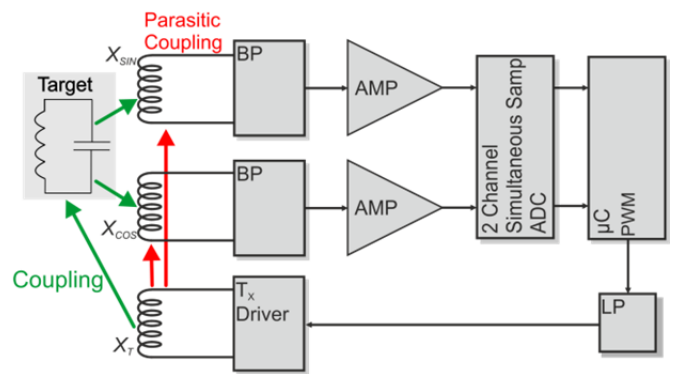


Figure 10. Functional block diagram of the signal condition electronic for the absolute or precise position receive coils.

four amplitude modulated receiver signals prior the quantization.

The demodulated and quantized envelopes of the absolute amplitude modulated signals can be represented as:

$$U_{QA}[i] = \frac{A_A}{2} \sum_{i=0}^{\infty} \sin\left(\frac{2\pi x(t)}{l_A}\right) \delta(t-iT), \quad (6)$$

$$U_{IA}[i] = \frac{A_A}{2} \sum_{i=0}^{\infty} \cos\left(\frac{2\pi x(t)}{l_A}\right) \delta(t-iT), \quad (7)$$

where δ is the Kronecker delta, U_{IA} and U_{QA} the in-phase and quadrature envelopes of the absolute receiver signals. Furthermore, the demodulated and quantized envelopes of the multi-cycle amplitude modulated signals can be represented as:

$$U_{QP}[i] = \frac{A_p}{2} \sum_{i=0}^{\infty} \sin\left(\frac{2\pi x_p(t)}{l_p}\right) \delta(t-iT), \quad (8)$$

$$U_{IP}[i] = \frac{A_p}{2} \sum_{i=0}^{\infty} \cos\left(\frac{2\pi x_p(t)}{l_p}\right) \delta(t-iT), \quad (9)$$

where U_{IP} and U_{QA} are the in-phase and quadrature envelopes of the multi-cycle receiver signals.

Due to the synchronized excitation, sampling, and processing of all the signals it is guaranteed that the receive coil signals $U_{A\sin}$, $U_{A\cos}$, $U_{P\sin}$, and $U_{P\cos}$ are sampled very close to their respective maximum thus yielding an optimal signal-to-noise ratio [11].

A second order RC-band-pass filter rejects signal components outside the band of interest $f_{in} = f \pm f_B = 1 \text{ MHz} \pm 50 \text{ kHz}$ before the modulated signals are sampled.

The argument $\arg\{U_{\Lambda}\}$ of the complex signal, $U_{\Lambda} = U_{IA} + jU_{QA}$ is computed digitally on a DSP to obtain the absolute position. This has to be also done for the multi-cycle coil. For arguments $\arg\{\cdot\} = m\pi/2$; $m = \{1, 2, 3, \dots\}$ the tangent used to calculate the phase exhibits singularities that need to be circumvented. Such singularities are avoided by use of a look-up table which uses the symmetry properties of the tangent and co-tangent functions by correctly selecting the quadrant, octant, and the tangent or cotangent part of $\varphi = 2\pi x(t)/l_A$ (see Figure 8). Therefore, the tan- and cotangent- functions are always bounded by ± 1 . The conditions for selecting the quadrant are given by:

$$Q_i = \begin{cases} i = 1, & \text{if } U_1 > 0 \wedge U_Q \geq 0 \\ i = 2, & \text{if } U_1 \leq 0 \wedge U_Q > 0 \\ i = 3, & \text{if } U_1 < 0 \wedge U_Q \leq 0 \\ i = 4, & \text{if } U_1 \geq 0 \wedge U_Q < 0 \end{cases} \quad (10)$$

which give a full position calculation of the target without any discontinuities at singular points [12].

5. MEASUREMENT SYSTEM AND PRELIMINARY MEASUREMENT RESULTS

Figure 10 illustrates the main components of the signal conditioning electronics for two receive coils. Each receive channel consists of a second order band-pass filter, an amplifier and a 12-bit ADC.

The two coarse and the two fine pitched receive channels are digitalized by a dual channel simultaneous sampling ADC. A DEV-BF537EDA-Lite eval board and the extender board EXT-BF5xx-AD/DA from Bluetechnix GmbH [13] provide the digital evaluation electronics, which sample at the same frequency as the carrier frequency f .

One end of the receive coils is connected to GND and the other is connected to a second order band-pass filter. The functional block diagram also shows a PWM generated transmit signal, but for the current measurement results and analysis, the excitation was done using an Agilent 33250A function waveform generator. The PWM excitation has not yet been implemented, but will be done in further development steps.

Figure 13 shows the single target test arrangement for precise absolute position measurement where the Isel linear translation stage with 17 μm minimum incremental motion, 20 μm repeatability accuracy and 90 cm travel can be seen. Furthermore, the test arrangement is able to move the target PCB off the measurement axis into the y-direction by a second linear translation stage with shorter travel to test the influence of lateral target to antenna misalignment. The antenna PCB is mounted on a perspex-glass bar and the target is mounted on a perspex-glass holder to get sufficient stand-off to electrically conductive and ferromagnetic materials. This offers to neglect eddy currents and makes possible to assume that the sensor coils are air-cored coils.

Figure 11 and Figure 12 show the demodulated receive coil

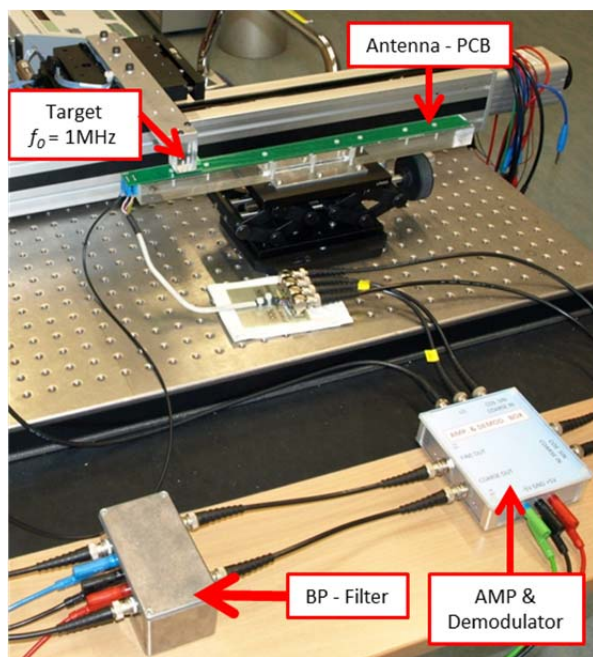


Figure 13. The picture shows a measurement setup of a high-frequency inductive position sensor for absolute linear position measurement. The used antenna design corresponds to the illustrated antenna PCB in Figure 1.

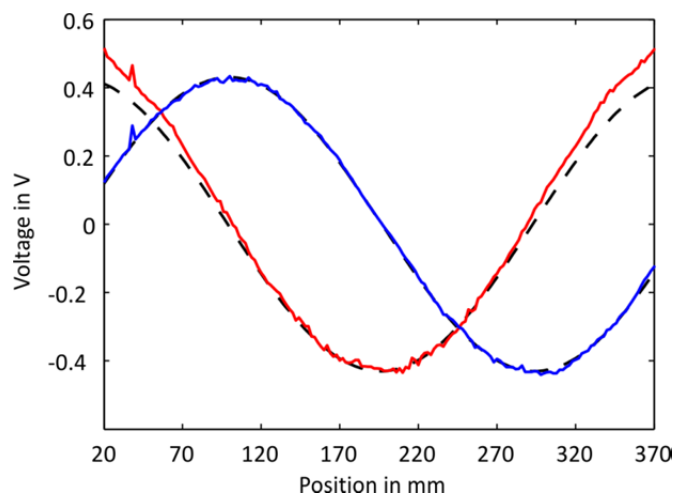


Figure 11. Demodulated output voltages U_{IA} (red) and U_{QA} (blue) of the two absolute receive channels compared to ideal sine and cosine (both black dashed) signals.

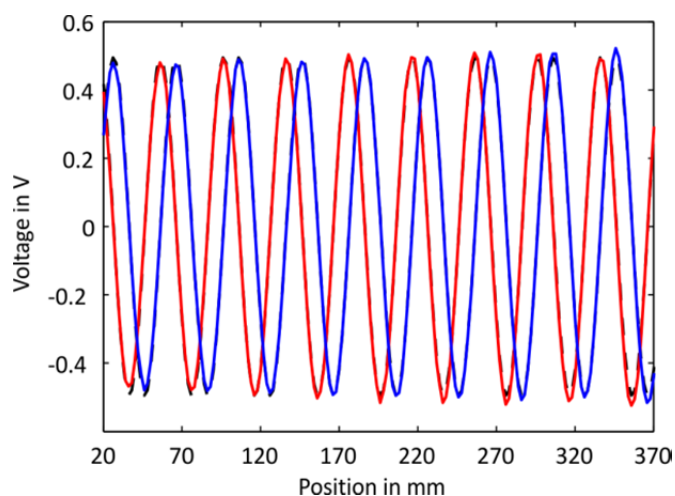


Figure 12. Demodulated output voltages U_{IP} (red) and U_{QP} (blue) of the two precise receive channels compared to ideal sine and cosine (both black dashed) signals.

signals over the full measurement range from 0 mm to 390 mm. These signals were obtained when the transmitter coil was excited by a 1 MHz sine wave signal with 4 V peak to peak. The demodulated and amplified by a factor 10 measured output voltages of the two absolute and precise position receive channels compared to ideal sine and cosine signals show the behavior of the target resonance circuit along the antenna PCB axis. The target PCB was shifted relatively to the antenna PCB by a linear stage, in 1 mm increments, from the current position to the new position along the antenna measurement axis. Furthermore, the voltage was measured at the cosine and sine coils for every position.

Figure 11 shows distortions at the beginning and at the end of the measurement range. Especially, the measured cosine-signal deviates from the ideal at both measurement range ends. These distortions occur due to the non-continued cosine structure by the straight track at the 0 mm and 390 mm measurement positions (see Figure 1).

The measured sine-signal fits much better to the ideal signal than the cosine-signal because its structure is not as prone to the edge effect as the cosine structure. Due to these distortions the practical measurement range is limited to approximately 80 % of the theoretical measurement range.

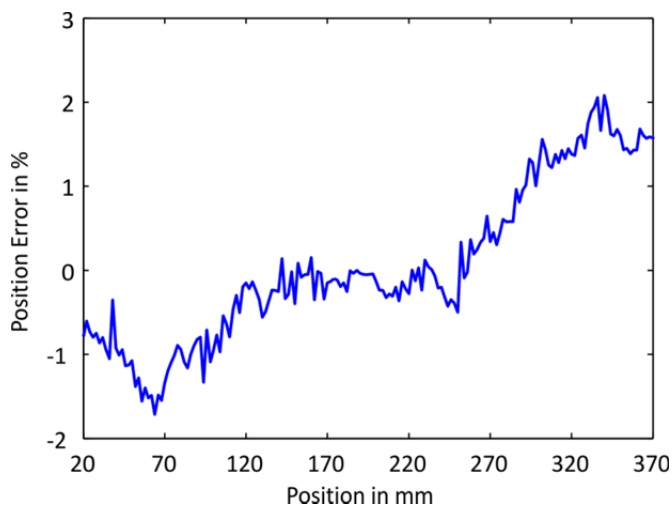


Figure 14. Position error of the absolute coils along the measurement axis.

The measured signals of the multi-cycle scale coils which are illustrated in Figure 12 behave almost like the ideal signals and distortions are barely to be seen. However, the amplitude increases slightly over the measurement range. This is due to an unintended decreasing target antenna gap over the measurement range in our experiment but due to the ratiometric principle the measurement uncertainty is affected only marginally.

Figure 14 and Figure 15 show the position error along the measurement axis over a range of 350 mm and approximately 90% of the theoretical absolute measurement length l_A is used by applying precise and absolute structures. Moreover, the preliminary measurement results show that the errors are smaller than 0.05 %. This corresponds to an absolute measurement error of approximately 190 μm .

6. CONCLUSION

An inductive position sensor based on PCB techniques which can operate in harsh environments has been presented. This sensor technology provides many advantages, for instance relatively wide measurement range, high resolution, reasonable production costs, and the ability to use PCB techniques, that offers supplier independency.

The measurement results clearly demonstrate that the sensor, offers a measurement error smaller than 0.05 % over 90 % of the theoretical measurement length without further digital signal processing. However, further analog and digital signal processing techniques reduce the measurement error by applying narrower band pass filters, type II servo loop or tracking observers. Active devices are not utilized, the resonant loop is passive and just a capacitance is used to tune the desired resonant frequency. The desirable properties contactless, absolute and non-optical make this sensor a good alternative to other linear sensors.

ACKNOWLEDGEMENT

The authors gratefully acknowledge the partial financial support for the work presented in this paper by the Austrian Research Promotion Agency and the Austrian COMET program supporting the Austrian Center of Competence in Mechatronics (ACCM).

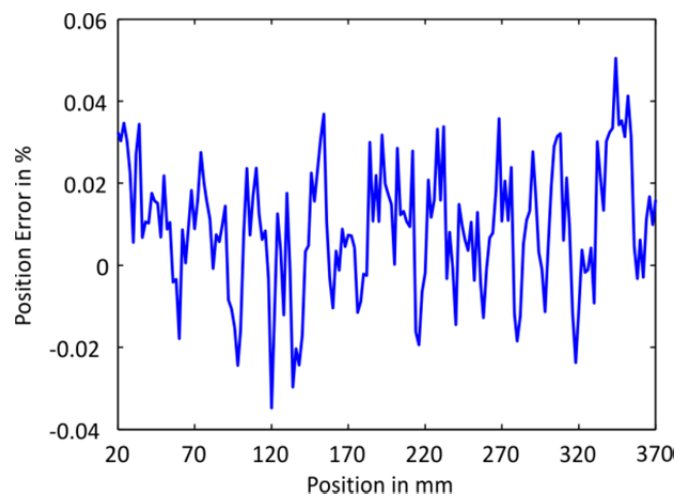


Figure 15. Position error of the multi-cycle coils along the measurement axis.

REFERENCES

- [1] M. Rahal, A. Demosthenous, An ASIC front end for planar high-frequency contact-less inductive position sensors, *Instrumentation and Measurement, IEEE Transactions on*, 58 (2009) pp.3021 –3030.
- [2] M. Rahal, A. Demosthenous, An integrated signal conditioner for high-frequency inductive position sensors, *Measurement Science and Technology*, 21 (2010) 015203 (12pp)
- [3] M. Rahal, A. Demosthenous, A synchronous chopping demodulator and implementation for high-frequency inductive position sensors, *Instrumentation and Measurement, IEEE Transactions on*, 58 (2009) pp.3693 – 3701.
- [4] J. Golby. Induktive Weg-Sensoren — Neues Messprinzip ermöglicht maßgeschneiderte Entwicklungen, *Elektronik*, 6 (2009),pp.22-26, www.elektroniknet.de/automation/sonstiges/artikel/28107/2.
- [5] B. Aschenbrenner, B. G. Zagar, DSP based read out system for contactless high-frequency inductive position sensors, *Proc. XX IMEKO World Congress, Busan, Republic of Korea, Sep. 2012*
- [6] R.-P. Jones, R. A. Doyle, M. A. Howard, D. A. James, D. Kreit, and C. S. Sils, Sensing apparatus and method, *US Patent No. 7208945 B2*, Apr. 24 2007.
- [7] P. Clayton, J. Mc Knight, Prediction of crosstalk involving twisted pairs of wires part II: A simplified low-frequency prediction model, *Electromagnetic Compatibility, IEEE Transactions on*, 21 (179), pp.105 – 114.
- [8] P. Clayton, *Introduction to electromagnetic compatibility*, Wiley-Interscience, Hoboken N.J., 2006, ISBN 0-471-75500-1
- [9] B. Aschenbrenner, B. G. Zagar, Planar High-Frequency Contactless Inductive Position Sensor, *IEEE International Instrumentation Conf.*, Minneapolis, USA, Mai 2013
- [10] R. B. Northrop, *Introduction to Instrumentation and Measurements*, 2013 Taylor & Francis, Boca Raton, 2005, ISBN 978-0-8493-3773-4
- [11] J. W. Howard, M. Graham, *High Speed Digital Design. A handbook of Black Magic*, Prentice Hall PTR , Englewood Cliffs NJ, 1993, ISBN 0-13-395724-1.
- [12] S. Sarma, V.K. Agrawal, S. Udupa, K. Parameswaran, Instantaneous angular position and speed measurement using a dsp based resolver-to-digital converter, *Measurement*, 41 (2008), pp.788 – 796.
- [13] Bluetechnix GmbH, www.bluetechnix.com/rainbow2006/site/blackfin_family/___dev___eval_boards/___dev-bf5xxda-lite/380/dev-bf5xxda-lite.aspx.